Proceedings World Geothermal Congress 2020+1
Reykjavik, Iceland, April - October 2021

Induced Seismic and Aseismic Slip in EGS Reservoir: Case Studies from Alsace, France

Olivier Lengliné, Léna Cauchie, Jean Schmittbuhl

EOST/IPGS, CNRS/Strasbourg University, 5 rue René Descartes, F-67084 Strasbourg, France

Jean.Schmittbuhl@unistra.fr

Keywords: Induced seismicity, EGS geothermal reservoirs, earthquake source properties, spectral analysis, repeating events

ABSTRACT

The injection of fluid in the upper crust, notably for the development or exploitation of geothermal reservoirs, is often associated with the onset of induced seismicity. Although this process has been largely studied, it is not clear how the injected fluid influences the rupture size of the induced events. Here we re-investigate the induced earthquakes that occurred during an injection at Soultz-sous-Forêts, France in 1993 and studied the link between the injected fluid and the source properties of the numerous induced earthquakes. We take advantage that deep borehole accelerometers were running in the vicinity of the injection site. We estimate the moment and radius of all recorded events based on a spectral analysis and classify them into 663 repeating sequences. We show that the events globally obey the typical scaling law between radius and moment. However, at the scale of the asperity, fluctuations of the moment are important while the radii remain similar suggesting a variable stress drop or a mechanism that prevents the growth of the rupture. This is confirmed by linking the event source size to the geomechanical history of the reservoir. In areas where aseismic slip on pre-existing faults has been evidenced, we observed only small rupture sizes whereas in part of the reservoir where seismicity is related to the creation of new fractures, a wider distribution and larger rupture sizes are promoted. Implications for detecting the transition between events related to pre-existing faults and the onset of fresh fractures are discussed. We also compare this behavior with those of other deep geothermal circulations in Northern Alsace, France (Soultz-sous-Forêts and Rittershoffen).

1. INTRODUCTION

While large induced events have to be avoid in order to guarantee safe operations of reservoir exploitation, small induced events still offer the opportunity to study the mechanical response of these fractured reservoirs submitted to intense perturbations. For instance, deep EGS geothermal reservoirs present a specific context for fault behavior analysis since they are at high temperature and relatively at low normal stress (reservoirs are typically shallower than 5 km depth at 150-200°C) (Cornet et al., 2007; Huenges & Ledru, 2011; Olasolo et al., 2016; Vallier et al ,2019). Indeed, this context favors the transition from frictionally stable or conditionally stable regime with velocity strengthening behavior to zones frictionally unstable with velocity weakening regimes that are responsible for seismic ruptures (Scholz 1998). It thus allows the investigation of the link between earthquakes and slowly deforming interfaces that are typically studied usually at much greater depth at the bottom of the seismogenic zone where the brittle-creep transition occurs (Beroza & Ide, 2011). Furthermore, because the imposed loading on the reservoir can be controlled from the wellhead injection rate or pressure and because a dense instrumentation can be deployed at proximity of the reservoir, it provides both information on the forcing term and high resolution observations on induced effects, both being favorable for a better knowledge of the fracture and fault behavior. It represents a large scale experiment (between the lab-scale and the scale of a developed fault system) that can help to decipher the links between fluid flow, slow aseismic movement and earthquake nucleation (Bernard, 2001).

Because most of the induced events related to injection in a geothermal reservoir have a small magnitude, capturing these events and achieving a detailed analysis of this seismicity, requires an appropriate instrumentation. Notably, borehole instruments, when available, provide a wealth of data compare to seismic surface network. This allows a better description of the ongoing deformation process that happens during the injection. Here we revisit the 1993 Soultz-sous-Forêts stimulation of the deep GPK1 well. This injection has been already extensively studied. It produced an abundant seismic activity (e.g. Cornet et al., 1997). A particular characteristic of this injection experiment is that repeated borehole imagery, before and after the injection, identified planar structures intersecting the borehole that slip aseismically (Cornet et al., 1997, Cornet, 2016). This was also confirmed from the analysis of the repeating earthquakes that took place on one of this structure whose cumulative slip matches the one observed from borehole measurement (Bourouis & Bernard, 2007). A dedicated network of borehole sensors was operating at the time of the injection providing a unique opportunity to see the details of the seismicity and to investigate the role of fluid on the source properties of the induced events (Baria et al., 1996).

Here we study the sources of the microseismic events that were recorded during the 1993 episode in order to detect any possible links between the source parameters of the seismic events and the injection history. In particular we investigate if the events possibly associated with aseismic slips within the reservoir have a distinct signature from the events that result from the creation of new fractures that appeared at later times and in a different part of the reservoir. For this, we first computed source properties for all events recorded, using a typical Brune's spectral model (Brune 1970). We then isolated repeating event sequences on individual asperities and obtained refined source parameters for these events. We show that the scaling of these events obeys globally the typical scaling law between radius, r, and moment, M_0. Interestingly, when events are analyzed at the scale of the asperity, this scaling law is not fulfilled and the moment M_0 is evolving independently of the radius r over a range that explains the typical broad dispersion of such (r,M_0) scaling law (Kanamori & Anderson, 1975). It suggests that an external factor is influencing the size of the seismic rupture at the asperity scale. We also observe that events size is on average changing over the course of the injection and for different parts of the reservoir. We interpret this control of the event size as a result of the fluid pressure on the rupture mode.

2. SEISMICITY DATABASE

We analyze the induced seismicity associated with the hydraulic stimulation of Soultz-sous-Forêts, France that occurred between September and October 1993 in two phases. The hydraulic stimulation was performed through the injection well GPK1. The injection process lasted from September 01, 1993 to October, 16th, 1993 with an interruption between September 17th and October 11th. The injection flow rate was increased by steps of 6 L/s every two days, reaching 36 L/s at the end of September episode and about 50 L/s at the end of October episode (Cornet et al., 1997). In total, approximately 44000 m3 of fluid was injected at a depth between 2850 and 3400 m (3550 m in October). About 15000 events were recorded by 3 accelerometers and 1 hydrophone installed in 4 deep wells (at depths between 1400 and 2000 m), in close proximity to the injection well, over the two months of the experiment. While the gap of seismicity between September 17th and October 11th is due to the injection shut in, several gaps of seismicity are observed on September 7th, 11th and 12th and are instead due to a loss of data. The accelerometers are 4-component instruments and have a flat response up to 1 kHz. The accelerometers were oriented with one vertical component and the other three are 109.5° away from each other and from the vertical direction. Conversion from 4 components to 3 components was performed during post-processing by Gaucher (1998). All seismic events were recorded on 2-second-long triggered windows and sampled with a frequency of 5 kHz. Event locations were firstly determined by the Camborne School of Mines Associates (Jones et al., 1995) from P and S waves arrivals and assuming an isotropic velocity structure. In a second step, relative location of events was performed based on travel time differences by Bourouis (2004). These latter locations are used in this study. As the stimulation starts, the seismicity is generated all around the injection source, at a depth of about 2950 m. The seismicity cloud grows gradually during the stimulation, with a distribution of events along sub-vertical planar structures (Cornet et al., 1997; Moriya et al., 2003; Evans et al., 2005). A few days after the stimulation started, the seismicity is observed to migrate principally to shallower depths (Cornet & Morin 1997). The final extent of the seismicity cloud reaches a distance of 800 m from the injection well at the end of the stimulation.

We first identified the P-wave arrival times for all events and at all stations through a STA/LTA approach (Earle & Shearer, 1994) applied to all signals filtered in a common frequency band between 80 and 270 Hz (STA=0.02 s, LTA=0.3 s and TH= 3.5). We then selected a 0.25-s-long signal window surrounding the P-arrivals (0.05 seconds before and 0.20 seconds after) and computed the acceleration amplitude spectra. The spectral energy of the events ranges between 80 Hz and 500 Hz for the stations 4550 and 4616 and hydrophone EPS1, and up to 270 Hz for the furthest station 4601. At higher frequencies, the spectral amplitudes decay rapidly due to the attenuation effect. We model the acceleration amplitude spectra of the events with the Brune's model (Brune, 1970) to estimate absolute values of the seismic moments M_0 and the corner frequencies f_c of each event. We use data from the seismic stations 4550 and 4616, the closest to the seismicity cloud and apply the analysis to the 80-500 Hz frequency band to hinder the noise contamination at lower frequencies and the attenuation effects affecting the higher frequencies. The source-receiver distances, r, are estimated from Bourouis (2004). Assuming a circular rupture model, we then infer the source dimensions from the corner frequency estimations through the following relationship from Madariaga (1976): $R = V_r/f_c$ with V_r is the rupture velocity taken as: V_r = 1069 m/s (Gaucher, 1998).

3. REPEATING EARTHQUAKES

3.1 Identification

We identify families of seismic events that are generated by repeated ruptures on the same asperity. These repeating events are not only characterized by highly correlated seismic waveforms but also by sharing a common source location and source mechanism. Forming families of repeating events allows us to use relative methods leading to more accurate estimates of the difference of source parameters. All changes that are resolved at the scale of the repeating earthquake sequence, are uniquely associated to temporal variation of the event sources. We identify those sequences of repeating events in a two-step procedure. We first gather events on the basis of high waveform cross-correlation (i.e. multiplets). We then select events in each family of similar waveform events, those that are co-located and reject events that are not. For this second step, we (i) estimate the source dimension through a spectral analysis; (ii) assess the inter-event distance from Δt_S - Δt_P time delays and (iii) verify that the event rupture areas of the sequence do overlap by checking that the source dimensions are larger than the inter-event distances.

We build a cross-correlation matrix where elements are given by the maximum of the cross-correlation function (CC) computed between two 0.55 s-long-windows (0.05 s preceding the STA/LTA picking time and 0.5 s after, or 2750 points long) of waveforms filtered between 80 and 270 Hz. This frequency band is chosen to maximize the signal-to-noise ratio of the recorded waveforms. The use of 0.55 s-long windows enables to encompass the P- and S-waves in the seismic waveforms. Since the analyzed signals are acceleration records, the resulting correlations emphasize the highest frequencies of the signal, compared to the use of correlations of velocity measurements.

We then cluster events according to the correlation coefficient computed from the vertical components for the stations that are the closest to the injection source (4550). The clustering threshold for the normalized correlation coefficient is set to 0.75. We test several correlation coefficient thresholds and keep 0.75 as a good compromise between a too weak selection of events that actually merges events of different sequences and a too tight selection that separates events that are part of a same sequence. We chose an open and non-exclusive algorithm for building clusters: in a set of events, only one connection (event pair with CC>0.75) is enough to cluster with other events. In this manner, 6970 events were classified into 1941 sequences of similar events.

We apply a spectral ratio method to compare corner frequencies and seismic moments between pairs of events of each sequence (Lengliné et al. 2014). The method provides relative information which has a higher accuracy than the comparison of absolute estimates using a Brune's spectral fitting of all individual event waveforms. At frequencies lower than fc, the spectral ratio is expected to be flat and its level is then used to estimate the relative moment of the events. We computed the spectral ratios in a common frequency range, 80-200 Hz, for all the repeating earthquakes. In this frequency range, the signal is indeed well above the noise level. We apply the spectral ratio technique to all pairs of events belonging to a common sequence. This produces a large amount of relative measurements (Δr and moment ratio) since radius and moment differences are computed for each possible pair of events in a sequence. To take advantage of this large set of data, we develop a minimization approach. Assuming as a priori information, the absolute

measurements of R and M_0 obtained from a Brune's spectral fitting and minimizing (in the least square sense) the relative measurements obtained from the spectral ratio method, we obtain high resolution values of R and M_0.

We estimate distances between earthquakes in each sequence of similar events through a high resolution cross-correlation analysis to get a fine measurement of S-P travel times (Poupinet et al., 1984; Bouchon et al., 2011). We assume that for each event pair of the sequence, their inter-distance is much smaller than the distance to the receiver. We slide a 128 sample-long window on the pair of signals along the entire signal duration, with steps of 64 samples. At each step, we compute a cross-correlation function between both signals and identify the time lag associated to the maximum of the function. We then determine ΔT_P and ΔT_S as the variation in P- and S- arrivals between the pair of events. This variation is zero when the two investigated events have an exact common origin. We compute ΔT_{S-P} for each pair of events in each sequence and by averaging the results on the three components and iterating for the three stations 4550, 4616 and 4601. For each event pair, we thus obtain three measurements, one corresponding to each station.

Finally, in each earthquake sequence, we compare the sum of the radii and the inter-event distance for each pair of events. An overlapping criterion is introduced and defined as an inter-event distance smaller than the sum of event pair radii. We only keep events in each sequence when their source overlaps with at least two other events of the sequence. This last criterion is useful to ensure that the so-formed repeating sequence represents a compact set of individual ruptures without mixing closely located but distinct repeating sequences. In this manner, we classified 4252 seismic events into 663 sequences comprising 3 or more repeating earthquakes (doublets are excluded in this selection).

3.2 Scaling of repeating events

We investigate here the moment-radius (R;M_0) scaling of all identified repeating events (see Figure 1). We first observe in this figure that repeating events have radii R, distributed between 2 and 13 meters and moments M_0 in the range [$3 \cdot 10^7$ - $3 \cdot 10^{10}$N m]. We however keep in mind that these absolute values depend on arbitrary parameters such as the rupture velocity but also on hypothesis such as the circular shape of the rupture zone (Aki, 1967; Kanamori & Anderson, 1975). The scaling between both parameters is expected to be of the form $M_0 \propto R^3$ as observed from numerous earthquakes worldwide (e.g., Kanamori & Anderson, 1975). We see from Figure 1 that globally the scaling is fulfilled and most events fall in a range of average stress drops between 0.2 MPa and 20 MPa. Again the absolute values of the stress drops are dependent on arbitrary choices like the rupture model and its parameters. We however observe that a dispersion of the stress drops exists.

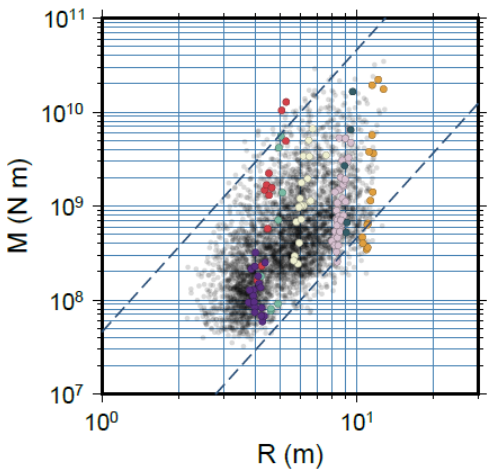

Figure 1: Seismic moments as a function of sources radii. The dashed lines represent constant stress drop values. The colored circles are attributed to individual sequences of repeating earthquakes (after Cauchie et al, 2020).

Interestingly, when we investigate at the scale of a single repeating earthquake sequence, we obtain a very different result. We show in Figure 1 several examples of repeating earthquake sequences using colored circles (one color per sequence). For each sequence, we observe a small variation of R for a large evolution of M_0, very differently from the classical scaling: $M_0 \propto R^3$. It has to be noted that the variation in moment within a repeating sequence is not a monotonic time evolution but is randomly distributed in time with no clear history of the moment evolution. When we are analyzing a single repeating sequence, we are dealing with relative measurements of the moment and radius variations that are well constrained and sensitive. It thus suggests that most of the dispersion around the theoretical moment-radius scaling is taking place at the scale of the repeating earthquake sequence itself.

3.3 Two populations of asperities

In order to look at the possible mechanisms that control the variations of the source parameters, we investigated how they do change over the course of the injection. Here we concentrate our analysis on the first part of the stimulation in September 1993 (from September 1st to September 20th). We report in Figure 2 the inferred radii of the repeating earthquakes as a function of time. We observe a spreading of the radii between 1 and 13 m. This spreading is actually increasing few days after the beginning of the injection (on September 6th, coincidentally with an increase of the flow rate) and then remains stationary during the rest of the stimulation. The average radius is also showing two regimes. We observed that during the first few days, most of the earthquakes have a small dimension (typically the inferred radius is rather constant around 4 m). In a second period, the average radius of the repeating earthquakes evolves to 6 m and shows a plateau for the rest of the stimulation.

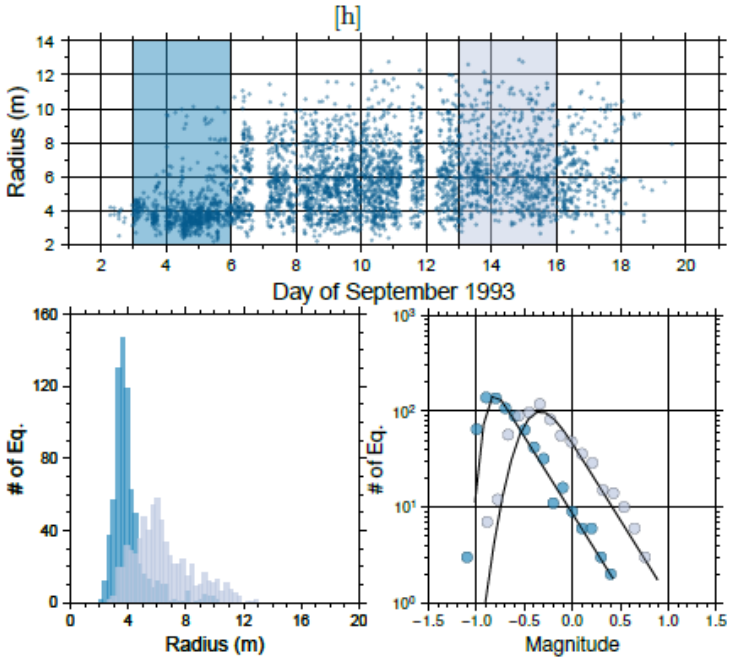

Figure 2: Top: Evolution of the source radius of all sequence events with time (blue circles). Two domains are identifed: one in dark blue at the beginning of the stimulation (2 days around Sept 5th) and one in light blue (2 days around Sept 14th). Bottom left: distribution of source radius for each period; Bottom right: distribution of the event magnitude, m for each period. Magnitudes are computed from m = 2/3 (log10(M_0) – 9.1) (Hanks & Kanamori, 1979).

We identified two representative periods of the same duration (2 days) during these two regimes: one around the 5th of September and one around the 14th of September. In Fig. 2, we detailed two properties of the repeating events during these two periods: the distribution of their radius and the distribution of their magnitude. During the first period, the radius distribution is peaked around 4 m which is significantly different from the second period when it appears larger and broader. Interestingly we observe that the magnitude distributions are similar as a Gutenberg-Richter power law distribution with the same b-values (b ~ 1:5 evaluated using the maximum-likelihood method of Ogata & Katsura (1993)) but a different prefactor (i.e. a-value). We conclude that there exists two populations of events that can be hardly distinguished by a b-value monitoring but better evidenced by a source radius characterization.

The transition between both periods dominated each by a specific population of repeating events (small and peaked for the first period and larger and broadly distributed for the second), is actually related to a specific transition in the flow rate history: the increase from 6 to 12L/s on September 6th, the 5th day of the stimulation. Indeed this transition corresponds to the increase of the average source radius from 4 to 6 m. When we compare this time evolution to the depth evolution of all the events, we see that at the transition from 12 to 18 L/s on Sept 8th, the seismicity starts to rise from the injection depth (2900m) to shallower zones (2000m deep). The transition has been interpreted as the onset and growth of a quasi-vertical fresh hydraulic fracture (Schmittbuhl et al. 2014; Cornet 2016). Here we show that the population of repeating events existing during the hydraulic fracture growth was existing before this 12-18 L/s increase, that is to say at the 6-12 L/s transition highlighting that the process of nucleating a new fresh fracture has started earlier. The average radius change is not related to a change in the proportion of repeating events in the whole population of seismic events. The Gutenberg-Richter distribution is characterized by two parameters for magnitudes M larger than the completeness magnitude: $P(M) = aM^{-b}$. We see a sharp increase of the a-value at the 6-12 L/s transition and fluctuations of the b-value around an average value of b 1.5. The b-value for the sequence events is typically slightly larger than for the whole seismicity. It confirms the result of Fig. 2 that each population of sequence events share a similar b-value but a different a-value.

3.3 Evolution of source parameters with time and depth

We see from Figure 3 that at the beginning of the injection, most of the seismicity is clustered at a depth around 2900 m. This depth corresponds to the upper limit of the open-hole section (2850-3400 m) where injection occurred. We observe that as the injection progresses, most of the earthquakes take place around a restricted depth range (2850-3150 m). They present a small source dimension as confirmed by the radius distribution that is peaked at 4 m independently of time and significantly different from distributions in other depth intervals. Immediately below this depth interval, in the depth range (3150-3500 m), repeating events are initiated later with a significant increase of the event size as a function of time. In the part of the reservoir just above the injection zone (2700-2850 m deep), a similar history is obtained. Earthquakes have a small radius (smaller than 5 m) at the beginning of the time series but show an abrupt increase of these event radii when the flow rate is increased from 6 L/s up to 12 L/s as discussed in the previous section. After this change of the flow rate, earthquakes in these two depth intervals, tend to have higher and broadly distributed radii dominated by the second population type of events. Finally the last depth interval we consider includes the upwards migration of the events towards shallower depth (2000-2700 m). This migration occurs after the increase of the flow rate to 18 L/s. These shallower events are the ones with the largest radius illustrating the second population of repeating events. No statistical change of radius is observed for these events from their first occurrences up to the end of the injection (Figure 3).

As a summary, we conclude that as the injection progressed we clearly evidence an increase of the source dimension of the earthquakes that occurred in the reservoir, but we observe that this increase does not occur everywhere in the reservoir: a) the depth section around the open hole (2850-3150 m) hosts mostly the first population of small and peaky distributed events over the whole course of the injection; b) the upper domain (2000-2700 m) corresponds to the second population of large and broadly distributed events; c) the two other domains show a mix between these two populations.

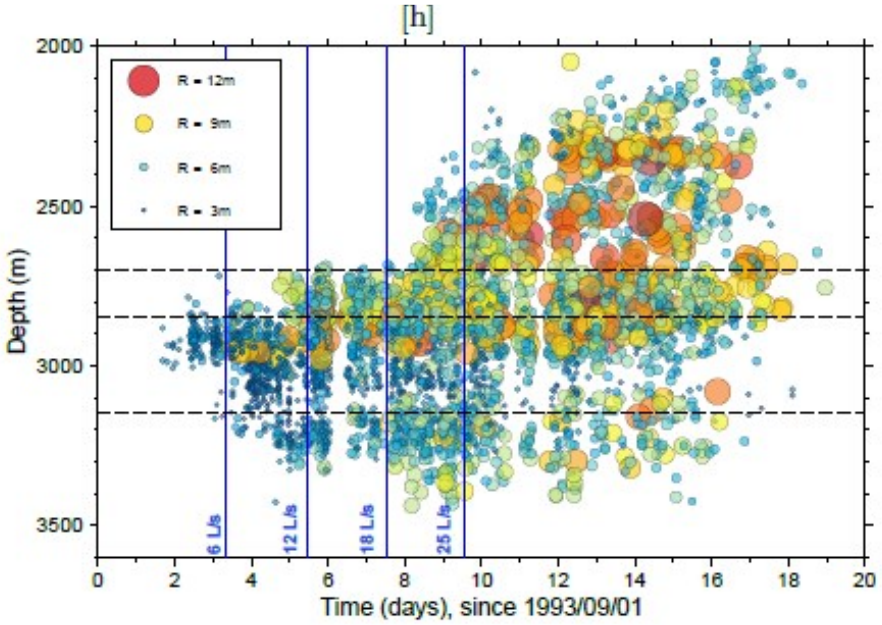

Figure 3: Evolution of the earthquake source sizes (radius of the rupture area) as a function of time and depth (color circles) (after Cauchie et al, 2020). Only events within identified sequences are reported. The size and color of the circles refer to the dimension of the event. The blue vertical lines represent the flow-rate steps. The horizontal dashed lines represent the various depth intervals chosen for analyzing the seismicity.

4. CONCLUSION

Based on accelerometer records of the 1993 injection experiment in the geothermal reservoir of Soultz-sous-Forêts, we estimated source parameters of repeating earthquakes. We show that the rupture area of these events is dependent on the mechanism at the origin of the seismicity. We first evidence that at the asperity level, a deviation from the typical scaling law between moment and radius is observed suggesting that the stress drop on each asperity is significantly fluctuating during a repeating sequence. We also show that the source radius of repeating events is a relevant feature for identifying two populations of events: a first population of small radius events is evidenced close to the injection well, in the zone of the reservoir that experienced aseismic slip on pre-existing faults. As the fluid pressure is increased in the reservoir and the seismicity develops farther away from the injection zone, a second population of repeating events emerges with a wider range of radii and a different recurrence behavior. We propose to relate this second population to the initiation of new large fractures that are fluid induced. Our results suggest that brittle and ductile mode of deformation promotes populations of repeating earthquakes that have distinct properties.

ACKNOWLEDGEMENTS

We thank F. Cornet, F. Cappa, P. Dublanchet, Z. Duputel, E. Gaucher, A. Zang, A. Jupe, J. Kinscher, G. Dresen, and L. Rivera for fruitful comments and suggestions. All date are available at CDGP (CDGP - Data Center for Deep Geothermal Energy) https://doi.org/10.25577/SSFS1993. The present work has been done under the framework of the LABEX ANR-11-LABX-0050-G-EAU-THERMIE-PROFONDE and benefits from a state funding managed by the French National Research Agency (ANR) as part of the 'Investments for the Future' program. It has also been funded by the EGS Alsace Grant from ADEME.

REFERENCES

Baria, R., Baumgartner, J., & Gérard, A., 1996. European hot dry rock programme 1992-1995.

Bernard, P., 2001. From the search of `precursors' to the research on `crustal transients', Tectonophysics, 338(3-4), 225-232.

Beroza, G. C. & Ide, S., 2011. Slow earthquakes and nonvolcanic tremor, Annual review of Earth and planetary sciences, 39, 271-296.

Bouchon, M., Karabulut, H., Aktar, M., Ozalaybey, S., Schmittbuhl, J., & Bouin, M.-P., 2011. Extended nucleation of the 1999 Mw 7.6 izmit earthquake, Science, 331(6019), 877-880.

Bourouis, S., 2004. Sismicité induite et comportement mécanique d'un massif granitique fracturé par injection d'eau. Application au site géothermique de Soultz-sous-Forêts, Ph.D. thesis, IPGP.

Bourouis, S. & Bernard, P., 2007. Evidence for coupled seismic and aseismic fault slip during water injection in the geothermal site of Soultz (France), and implications for seismogenic transients, Geophysical Journal International, 169(2), 723-732.

Brune, J., 1970. Tectonic stress and the spectra of seismic shear waves from earthquakes, Journal of Geophysical Research, 75(26), 4997-5009.

Cauchie, L., Lengliné, O., & Schmittbuhl, J., 2020. Seismic asperity size evolution during fluid injection: case study of the 1993 Soultz-sous-Forêts injection, Geophys. J. Int., 221, 968–980, doi: 10.1093/gji/ggaa051.

Cornet, F., Bérard, T., & Bourouis, S., 2007. How close to failure is a granite rock mass at a 5 km depth?, International Journal of Rock Mechanics and Mining Sciences, 44(1), 47-66.

Cornet, F. & Morin, R., 1997. Evaluation of hydromechanical coupling in a granite rock mass from a high-volume, high-pressure injection experiment: Le Mayet de Montagne, France, International Journal of Rock Mechanics and Mining Sciences, 34(3-4), 207.

Cornet, F. H., 2016. Seismic and aseismic motions generated by fluid injections, Geomechanics for Energy and the Environment, 5, 42 - 54.

Earle, P. & Shearer, P., 1994. Characterization of global seismograms using an automatic-picking algorithm, Bulletin of the Seismological Society of America, 84(2), 366-376.

Evans, K., Moriya, H., Niitsuma, H., Jones, R., Phillips, W., Genter, A., Sausse, J., Jung, R., & Baria, R., 2005. Microseismicity and permeability enhancement of hydrogeologic structures during massive fluid injections into granite at 3 km depth at the Soultz hdr site, Geophysical Journal International, 160(1), 388-412.

Gaucher, E., 1998. Comportement hydromécanique d'un massif fracturé: apport de la micro-sismicité induite. Application au site géothermique de Soultz-sous-Forêts, Ph.D. thesis, IPGS-Paris Diderot.

Huenges, E. & Ledru, P., 2011. Geothermal energy systems: exploration, development, and utilization, John Wiley & Sons.

Jones, R., Beauce, A., Jupe, A., Fabriol, H., & Dyer, C., 1995. Imaging induced seismicity during the 1993 injection test at soultz-sous-forêts., in World Geothermal Congress. International Geothermal Association, pp. 2665-69.

Kanamori, H. & Anderson, D., 1975. Theoretical basis of some empirical relations in seismology, Bulletin of the Seismological Society of America, 65(5), 1073.

Lengliné, O., Lamourette, L., Vivin, L., Cuenot, N., & Schmittbuhl, J., 2014. Fluid-induced earthquakes with variable stress drop, Journal of Geophysical Research: Solid Earth, 119(12), 8900-8913.

Madariaga, R., 1976. Dynamics of an expanding circular fault, Bulletin of the Seismological Society of America, 66(3), 639-666.

Moriya, H., Niitsuma, H., & Baria, R., 2003. Multiplet clustering analysis reveals structural details within the seismic cloud at the Soultz geothermal field, France, Bulletin of the Seismological Society of America, 93(4), 1606-1620.

Olasolo, P., Juarez, M., Morales, M., Liarte, I., et al., 2016. Enhanced geothermal systems (egs): A review, Renewable and Sustainable Energy Reviews, 56, 133-144.

Poupinet, G., Ellsworth, W., & Frechet, J., 1984. Monitoring velocity variations in the crust using earthquake doublets: An application to the Calaveras fault, California, Journal of Geophysical Research: Solid Earth, 89(B7), 5719-5731.

Scholz, C. H., 1998. Earthquakes and friction laws, Nature, 391(6662), 37.

Vallier, B., Magnenet, V., Schmittbuhl, J., & Fond, C., 2019. Large scale hydro-thermal circulation in the deep geothermal reservoir of soultz-sous-forêts (france), Geothermics, 78, 154-169.